Femoral Fracture Type can be Predicted from Femoral Structure:

A Finite Element Study validated by Digital Volume Correlation Experiments.

M. Ikhwan Z. Ridzwan[1,2], Chamaiporn Sukjamsri[1,3], Bidyut Pal[1,4], Richard J. van Arkel[1],

Andrew Bell[5], Monica Khanna[6], Aroon Baskaradas[7], Richard Abel[8], Oliver Boughton[8], Justin

Cobb[8], and Ulrich N. Hansen[1]

[1]Department of Mechanical Engineering, Imperial College London, London SW7 2AZ, UK

[2]School of Mechanical Engineering, Engineering Campus, Universiti Sains Malaysia, 14300

Penang, Malaysia

[3]Department of Biomedical Engineering, Faculty of Engineering, Srinakharinwirot University,

Nakhonnayok, 26120, Thailand

[4]School of Engineering, University of Portsmouth, Portsmouth, PO1 3DJ, UK

[5]MSC Software Ltd., 4 Archipelago, Lyon Way, Frimley, Surrey GU16 7ER, UK

[6]Department of Clinical Imaging, Imperial College Healthcare NHS Trust, London, UK

[7]Trauma and Orthopaedic Surgery, Imperial College Healthcare NHS Trust, London, UK

[8]Department of Surgery and Cancer, Imperial College London, Charing Cross Hospital, London

W6 8RF, UK

1

ABSTRACT

Proximal femoral fractures can be categorised into two main types: neck and intertrochanteric fractures accounting for 53% and 43% of all proximal femoral fractures, respectively. The possibility to predict the type of fracture a specific patient is predisposed to would allow drug and exercise therapies, hip protector design and prophylactic surgery to be better targeted for this patient rendering fracture preventing strategies more effective. This study hypothesized that the type of fracture is closely related to the patient-specific femoral structure and predictable by finite element (FE) methods. Fourteen femora were DXA scanned, CT scanned and mechanically tested to fracture. FE-predicted fracture patterns were compared to experimentally observed fracture patterns. Measurements of strain patterns to explain neck and intertrochanteric fracture patterns were performed using a digital volume correlation (DVC) technique and compared to FE-predicted strains and experimentally observed fracture patterns. Although loaded identically, the femora exhibited different fracture types (6 neck and 8 intertrochanteric fractures). CT-based FE models matched the experimental observations well (86%) demonstrating that the fracture type can be predicted. DVC-measured and FE-predicted strains showed obvious consistency. Neither DXA-based BMD nor any morphologic characteristics such as neck diameter, femoral neck length or neck shaft angle were associated with fracture type. In conclusion, patient-specific femoral structure correlates with fracture type and FE analyses were able to predict these fracture types. Also, the demonstration of FE and DVC as metrics of the strains in bones may be of substantial clinical value, informing treatment strategies and device selection and design.

INTRODUCTION

Proximal femoral fractures (PFF) can be categorised into two main types: femoral neck (intracapsular) and intertrochanteric (extracapsular) fractures accounting for 53% and 43%, respectively, of all PFF [1]. Each fracture type is treated with a specific type of operative treatment and has different potential complications to patients [2]. The ability to assess which fracture type a specific patient is predisposed to could aid fracture prevention strategies. It has been shown that by selecting specific exercise regimes [3; 4] or drug treatments [5] specific parts of the femoral structure can be targeted and strengthened, potentially reducing the risk of this fracture type. Hip protectors could be designed to preferentially protect against the type of fracture the specific patient is prone to. More controversially, knowledge of the likely fracture type could aid prophylactic surgery.

Several studies have been performed to identify the factors that determine the fracture type [6-16]. A summary of these studies suggests that intertrochanteric fractures were associated with femora with lower bone mineral density (BMD) and thinner cortices while femoral neck fractures were associated with structural features such as a higher neck shaft angle (NSA) and a longer femoral neck length (FNL). However, these findings were not consistent, often reporting no significant effects, and some of the results were contradictory. Most of these studies were clinical studies involving patients who had suffered a fracture. The results of such studies are difficult to interpret in terms of the structural features of the femur associated with the fracture type as other factors, such as fall direction [17], will also have an effect on the resulting fracture type.

To determine if the femoral structure alone predisposes a patient to a particular type of fracture this study aimed to isolate femoral structural features from other characteristics that may affect the

64   fracture type. To this end, cadaveric femora were tested under identical laboratory conditions,

65   simulating a fall to investigate if these femora would exhibit different fracture types.

66

67   Any fracture has a degree of randomness resulting in a distribution of strength values. Thus the

68   fracture type, may also have a seemingly random nature, the source of which may not be

69   discernible from the overall structure assessed visually or from a CT scan. Hence, a CT based finite

70   element (FE) analysis of each of the specimens was also carried out. The FE method is a frequently

71   used tool for investigating femoral fracture load [12; 17-22] and its particular advantage in the context

72   of our study is that it is entirely deterministic, containing no random elements. Thus, if the FE

73   analysis predicts the experimental fracture types, then the fracture type is not determined by

74   random effects but from features contained within the CT scan.

75

76   The hypothesis of this paper is that the femoral structure, including bone density distribution, as

77   discernible from a CT-scan, determines if a patient is more predisposed to a femoral neck than to

78   an intertrochanteric fracture. As part of the investigation it was assessed if the FE methodology

79   could predict these fracture types. Thus, we assessed if FE may be used as a clinical tool for

80   predicting the fracture type and aid in treatment planning. Finally, it was investigated if femoral

81   characteristics, such as local BMD or femoral neck axis length, were associated with the fracture

82   type.

83

MATERIAL AND METHODS

Femur Specimens and Preparation

Fourteen human cadaveric femora from eleven donors were obtained from Platinum Medical, Biological Resource Center, Phoenix, USA. The donors (mean age, 66.5±14.5 years; range: 42-86 years) were four males, specimens M1 to M4, and seven females, specimens F1 to F10. This study was approved by the National Research Ethics Service (NRES) Committee London − London Bridge, United Kingdom (Ethics reference number: 12/LO/0797). The soft tissues were removed from the femora, and all femora were cut approximately 15 cm from the distal articular surface. The specimens were stored at -20°C and thawed to room temperature for specimen preparation as well as prior to dual energy X-ray absorptiometry (DXA), CT scanning and mechanical testing.

Imaging Methods

The femora were radiographed, CT and DXA scanned. CT images were used for generating 3D FE models. Radiographs were used for measuring femoral geometrical characteristics while the DXA measurements were used to quantify BMD. Femora were scanned with a Philips, 64 slice CT scanner. The slice thickness was 1 mm. The settings were 120kV, 70mAs, and a 512 x 512 pixels image matrix with pixel size between 0.8 to 1.0 mm. In-vitro DXA scans of the cadaveric femora, submerged in a water bath and positioned to replicate the routine clinical practice of supine patient position with the femur in 20-25° of internal rotation, were performed using GE Lunar Prodigy.

In-Vitro Mechanical Testing

The mechanical testing to fracture of the 14 femora was divided into two parts, twelve of the femora were tested in Part 1, while the remaining 2 femora, F7 and F10, were tested in Part 2. The mechanical set-up in Part 1 and Part 2 was conceptually the same (Figure 1), only the set-up in Part 2 was modified to be placed within a CT scanner, enabling CT scanning of the loaded specimen. In Part 1 the purpose was simply to record the fracture type and fracture load. In Part 2, in addition to recording to the fracture type and load, the specimen was CT-scanned at incrementally increasing loads until final failure. These CT scans were analysed using Digital Volume Correlation analysis (DVC) which measures the increasing strains within the femur during loading by tracking the grey scale patterns within the CT images as these patterns are deformed during loading. The main purpose of Part 2 was to provide strain fields close to fracture which could be used to further validate the FE fracture simulation.

Part 1: In-Vitro Mechanical Testing within an Instron Test Machine

To represent a sideways fall configuration each femoral shaft was positioned 10° from horizontal and the femoral neck axis internally rotated by 15° relative to a vertical axis (Figure 1) [23-25]. The femur was fixed at the distal end allowing the distal end to rotate freely around the axis normal to the plane of Figure 1. The medial aspect of the femoral head and the lateral aspect of the greater trochanter were covered with PMMA to prevent local crushing and simulating the effect of soft tissue cover [24]. Each femur was loaded to failure defined as the peak of the load-deformation curve using an Instron 8874 testing machine (Instron Corporation, Canton, MA). A constant vertical displacement of 6.6 mm/s was applied to the femoral head which rested on an x-y table to eliminate

126 any reaction forces. Load and displacement data were sampled at 1000 Hz. The load was measured

127 using a uniaxial load cell. This load cell had a full-range of ±10 kN and was accurate to 0.5% of

128 the indicated load.

129

130 **Part 2: In-Vitro Mechanical Testing within a Clinical CT Scanner and DVC Strain Analysis**

131 In part 2 a CT-compatible custom-designed loading device was used. The set-up was conceptually

132 the same as in Part 1 but the load was introduced by turning a Hex screw and measuring the load

133 using a compression load cell (LBM-1000, Interface Force Measurements Ltd.) (Figure 1). The

134 device was designed and positioned within the CT scanner in such a way that there were no metal

135 components in the field of the CT scan thereby avoiding metal artefacts in the images. Patient scan

136 settings of 120 kVp and 60 mAs were used. The compressive load was applied to the femoral head

137 in increments of approximately 500 N. At the end of each increment a CT scan was performed. To

138 reduce stress relaxation effects during the 4.4 seconds of the CT scan the specimen was held for 5

139 minutes prior to scanning which allowed the load to stabilise and no change in load could be

140 detected during the scan. This process of incremental loading and CT imaging was continued until

141 final failure.

142

143 DVC uses digital image tracking to determine the displacement of patterns of voxel grey scale

144 values in two sequential CT images of bone under increasing load. As the method utilises CT

145 scans, the DVC method has the ability, uniquely amongst experimental methods, to assess the

146 internal strains in bone [26-28]. Previous studies were based on micro-CT imaging and a novel aspect

147 of this study was the use of DVC based on clinical CT images. The CT image files were imported

148 into commercial DVC software (DaVis 8.1.6, LaVision, Goettingen, Germany). Two scans were

149 taken at zero load and confirmed that the maximum noise levels were 0.0003 and   -0.0005 for

150 the maximum and minimum strains, respectively, which had a negligible effect on the measured

151 strain values. Software settings were: subvolume size sequences of 96x96x96, 76x76x76, and

152 48x48x48 voxels/mm, 75% overlap and a correlation degree of 0.94. The software calculated the

153 distribution of principal strains throughout the loaded femur. The DVC-measured strain

154 distributions were compared with the FE-predicted strain patterns and the fracture patterns

155 observed during mechanical testing.

156

157 **FE Model of Proximal Femur**

158 The CT dataset of the cadavers were segmented using medical image analysis software (Avizo,

159 Version 6.3, Visualization Sciences Group, Burlington, MA, USA). The datasets had an average

160 of 280 CT slices that covered the proximal head to about 25 cm down the shaft of the femur from

161 the greater trochanter. Surface models were generated and exported to the FE software

162 (Marc/Mentat 2013, MSC Software Corp., Santa Ana, CA, USA) to develop three-dimensional FE

163 models of the femur. The models were meshed using linear 4-node tetrahedral solid elements.

164 Mesh convergence analyses of three key results were performed: the load to initiation of failure

165 (prior to deactivation of elements); the ultimate fracture load and the predicted fracture type. The

166 converged meshes contained approximately 70,000 nodes and had an average element edge length

167 of 1.3 mm (Figure 2).

168 Bone was modelled as a linear and isotropic material. The elastic modulus of each bone element

169 was determined from the Houndsfield Units (HU) of the CT image using a previously established

170   procedure [29]. Specifically, the bone apparent density (ρ_{app} in g/cm^3) was calculated using a linear

171   relationship $\rho_{app} = 0.00089\ HU + 0.035$ and the Young's Modulus from $E = 6.850\ \rho_{app}^{1.49}$. A

172   Poisson's ratio of 0.3 was assumed.

173

174   The FE closely simulated the experimental set-up in Figure 1. The distal end was fixed apart from

175   rotation around the axis normal to the plane of Figure 1. Nodes corresponding to the area covered

176   by PMMA in the experiments (the trochanteric area) were constrained in the vertical direction.

177   The vertical load applied to the surface of the femoral head was distributed on nodes over an area

178   of approximately 3 cm in diameter. Femoral failure was predicted using maximum/minimum

179   principal strain criteria. The maximum and minimum principal strains to failure used for both

180   cortical and cancellous bone were 0.62% and -1.04%, respectively [30; 31].

181

182   Assessing the FE-predicted fracture type based on just one element or a small area that first reaches

183   the critical failure threshold was not considered sufficiently accurate since an initial failure may

184   get arrested with subsequent failure initiating in another region of the femur. For these reasons a

185   progressive FE failure simulation was adopted. Elements that met the principal strain failure

186   criterion mentioned earlier were considered failed and automatically deactivated from the analysis

187   during the iterative solution procedure (Figure 2). The use of iterative-level, load stepping

188   constraints in Marc ensured convergence during the deactivation. A Newton-Raphson iterative

189   scheme was used which meant that the onset of complete failure was numerically indicated by a

190   reduced load in a subsequent increment.

191

Definition of Fracture Types

In both the physical experiment and in the FE models the specimens were tested until peak load which coincided with major but not complete fracture of the bone and as a result fractures were never displaced. A fracture that was contained within the intracapsular region (including subcapital and any variation of a fracture of the cervical neck) was defined as a neck fracture whilst a fracture that was contained within the extracapsular region (including fractures that were limited to or involved the greater trochanter, lesser trochanter, intertrochanteric region and subtrochanteric fractures) was defined as an intertrochanteric fracture. Fractures at the interface of the two regions (involving the basicervical region and extending outside the capsule into the intertrochanteric region running parallel to the basicervical region) were also categorised as intertrochanteric fractures due to these fractures being treated as extracapsular fractures in the clinical setting [32]. The classification of fractures was carried out blinded by three independent observers (MIZR, OB, & UNH); in cases of disagreement, the fracture type was classified according to the majority.

Femoral Characteristics

From DXA scans and 2D anterior-posterior radiographs (Figure 3) of the 14 specimens the total BMD, neck BMD, Ward's triangle BMD, greater trochanteric BMD, isthmus cortical index (CI), neck diameter (ND), femoral neck length (FNL) and neck shaft angle (NSA) were measured to determine which, if any, parameters were associated with fracture type.

Statistical Analysis

213 Inter-rater reliability was assessed using Fleiss' kappa [33]. All other data were analysed in SPSS

214 (version 22, SPSS Inc., Chicago, Illinois) with the significance level set at $p < 0.05$. First, the

215 correlation between the measured experimental fracture load and both BMD and FE-predicted

216 fracture load was assessed with Pearson's product-moment correlation. Then the data were split

217 into the two fracture groups, neck fracture or intertrochanteric and a Fisher's Exact Test was used

218 to assess the association between the FE-predicted fracture types and the observed experimental

219 fractures types. Finally, differences between specimen characteristics of the two fracture groups

220 were analysed with unpaired t-tests.

221

222 **RESULTS**

223 The experimental and FE-predicted fracture loads and types are listed in Table 1 which also shows

224 the total BMD values for each sample. Fracture load for specimen M4 was not recorded due to a

225 technical error when collecting data and was not included for correlation statistics. Specimen M1

226 was identified as a potential outlier as it had a BMD 1.5 times the interquartile range greater than

227 the upper quartile of other specimens. A patient with such dense bone is unlikely to fracture and

228 hence correlation data is presented both with and without this specimen. As expected, there was a

229 strong correlation between increasing BMD and increasing experimental fracture load ($r = 0.82$

230 with M1, $r = 0.63$ without M1, p < 0.029 both with and without M1; Figure 4). There was an even

231 stronger correlation between increasing FE-predicted fracture load and increasing experimental

232 fracture load ($r = 0.90$ with M1, $r = 0.75$ without M1, $p < 0.005$ both with and without M1, Figure

233 4). The FE model predicted the experimentally observed fracture type 86 % of the time (Table 2,

234 95 % CI: *65-100 %*, Fisher's Exact $p = 0.026$). The inter-rater reliability (Fleiss' kappa) for

235 assessing these fracture types was 0.95.

236

237 The fracture types that occurred in the experimental rig were consistent with the FE-predicted and

238 DVC-measured strain patterns (Figure 5). The two specimens that were used for this DVC analysis

239 had notably different bone quality. F7 was osteopenic (T-score: -2.1) and F10 was osteoporotic

240 (T-score: -4.3) and the two specimens exhibited different fracture types. The DVC strain

241 measurements show the strain just prior to fracture and, consistent with the FE predictions and

242 experimental fracture type, high strain concentrations can be noted in the neck and trochanteric

243 regions, respectively. The FE and DVC assessments of strain were remarkably similar in regards

244 to qualitative patterns as well as quantitative values. Thus, DVC strain measurements corroborated

245 the FE predictions, both seemingly able to explain the fracture type.

246

247 No anatomic element was able to distinguish between fracture types in this small study (Table 3).

248 No differences in any BMD measurements at any locations were detected between the fracture

249 groups; neither for the entire group (all $p \geq 0.08$), or for female only specimens (all $p \geq 0.07$).

250 However, there was a trend that specimens that fractured in the intertrochanteric region failed at

251 lower loads, and had lower BMD than those that fractured at the neck. No other difference between

252 the two fracture-groups were detected for any of the other variables: gender, age, height, weight,

253 BMI, Isthmus CI, neck diameter, FNL and NSA; neither for the entire group (all $p \geq 0.21$), nor for

254 female-only specimens (all $p \geq 0.21$).

255

DISCUSSION

This study investigated whether the femoral fracture type was random or if it could be predicted from the femoral structure based on a CT scan. Femora loaded in an identical manner resulted in a mix of fractures (6 neck fractures and 8 intertrochanteric fractures) reflecting clinical reality [1], and giving credibility to the experimental set up. DXA-scores correlated well with the energy required to cause a fracture confirming the relevance of this imaging modality in the assessment of fracture risk. However, DXA was unable to distinguish between the types of fracture – no statistically significant differences were found between the fracture groups and BMD. In contrast, the FE model accurately predicted both the fracture load and the fracture pattern.

Keyak, et al. [12] and Pulkkinen, et al. [9] also reported a mix of fracture types when testing cadaver femora loaded in an identical manner (10 neck versus 4 intertrochanteric and 88 neck versus 51 intertrochanteric fractures, respectively). Keyak, et al. [12] and Koivumaki, et al. [8] compared FE-predicted fracture types to in-vitro cadaver fracture types and found degrees of matching of 79% and 85%, respectively, supporting the predictive capability of FE found in our study.

In contrast to the FE modelling approaches by Keyak, et al. [12] and Koivumaki, et al. [8] our study modelled the progression of fracture from initiation to final failure. Keyak et al. predicted only the initial failure of a small area. If this area coincided with any part of the much larger experimentally observed fracture region it was considered a match. Such a strategy is likely to over-predict the degree of matching. Koivumaki et al. did not predict fracture but related the strain in the greater trochanteric region to the strain in the neck region. The region with the larger strain was predicted

278   to fracture. While our approach of simulating the progressing fracture and comparing like with

279   like (fracture type with fracture type) did not vastly improve the degree of matching over those

280   earlier studies it may arguably be more reliable.

281

282   The FE models statistically explained 57% of the variability seen in experimental fracture loads

283   whereas DXA BMD-measurements were only able to explain 39% of the variability (Figure 4).

284   These findings are consistent with Cody, et al. [34] and Orwoll, et al. [35] who also found FE to be

285   superior in this aspect and to the findings of Cheng, et al. [36] who reported an R^2 value of 0.76

286   between total BMD and femoral strength. Cheng et al. also report femoral strengths (3.98kN ±

287   1.6kN) which are comparable to the results of our study.

288

289   Mautalen, et al. [15], in a comprehensive review of clinical studies, reports low BMD to be associated

290   with intertrochanteric fractures. However, Dretakis, et al. [37] and Maeda, et al. [7] did not find a

291   significant effect and Pulkkinen, et al. [9] reports lower strength (closely related to low BMD) to be

292   associated with neck fractures. In our study, the intertrochanteric group had a nominally lower

293   BMD (Table 3) which would be consistent with most previous studies, however, this result was

294   not statistically significant. Our finding may be a type II statistical error due to the low power of

295   the study as discussed below. The fact that the FE methodology, which includes any effect of low

296   BMD, and despite the low power of the study exhibited a strong ability to predict the fracture types

297   indicates the strength of this method over DXA.

298

299 Cheng, et al. [36] reported neck, Ward's triangle and greater trochanteric BMD values in females of

300 0.676 g/cm^2, 0.515 g/cm^2 and 0.612 g/cm^2, respectively, which compares reasonably with the

301 values found in our study (Table 3). Previous studies have reported an association between the

302 location of BMD and the fracture type; low neck BMD being associated with neck fractures [6] and

303 low trochlear BMD being associated with intertrochanteric fractures [11; 15], while Maeda, et al. [7] did

304 not find a significant association. In our study we also did not find such an association. Maeda, et

305 al. [7] did find that a low Isthmus CI, suggested to reflect a general thinning of the cortices including

306 the neck and trochanteric regions, was associated with intertrochanteric fractures. In our study we

307 did not find such an association. However, the cortices at the isthmus were approximately 8 mm

308 thick and considering the CT scan voxel dimension of ~ 1 mm it may be that the inaccuracy of our

309 measurements prevented us from finding an association.

310

311 Pulkkinen, et al. [9] reported ND, FNL and NSA values for females with neck fractures of 3.06 cm,

312 9.7 cm and 126°, respectively, which compares well with the values found here (Table 3). A wide

313 and short femoral neck, and a low neck shaft angle all theoretically strengthen the femur against a

314 femoral neck fracture and predispose the femur towards an intertrochanteric fracture. Such

315 associations have been reported previously [7; 11; 14] although in other studies such associations were

316 not found Dretakis, et al. [37]. In our study we did not find an association between these parameters

317 and fracture type.

318 An important limitation affecting all the above findings was the limited number of samples.

319 Notably, any differences in fracture strength and BMD values failed to differentiate statistically

320 between the fracture groups. However, the p-values for these analyses were not far from the

321   statistical significance threshold of 0.05 (Table 3). Another limitation of the study was the

322   subjective judgment made when classifying fractures into neck or intertrochanteric fracture.

323   However, the three observers assessed the fracture types with inter-rater reliability of 0.95,

324   suggesting that the reliability of the classification was not a severe limitation.

325

326   We used a loading rate of 6.6 mm/s comparable to that used in similar studies[18; 38; 39] but much

327   lower than the loading rate during a sideways fall of ~100 mm/s[23]. Courtney et al. (1994)[23] found

328   that fracture load increased but energy to fracture was unaffected by loading rate. As the energy to

329   fracture was unaffected it seems likely that also the fracture type would be unaffected by loading

330   rate. Based on Courtney's work, we expect that our study underestimated the fracture load by about

331   20% but did not change the fracture type.

332

333   There are several limitations of the FE modelling that may explain why 14% of fracture types were

334   not predicted accurately. The FE model did not include features that are not captured by the CT

335   image such as the presence of microcracks, differences in bone mineral crystallinity, or changes

336   in bone collagen with age. The effect of such factors on the resulting fracture type will appear

337   random in the context of the FE model used in this research. Another notable uncertainty involves

338   details to reflect the real conditions of the impact to the greater trochanter during a fall (a

339   complexity shared with the experimental set-up). However, too rigid or blunt a support would lead

340   to high rates of trochanteric fractures which we did not find and may indicate that the effect of this

341   limitation is minor. Finally, the fracture of bone is likely to be affected by the anisotropic

342   mechanical properties of bone, including strength, which was not simulated.

343

Although initially introduced as a validation tool for the FE-predicted strains, the DVC component is an important additional outcome of the study. The DVC measured the strains throughout the bone and showed areas of critical strains indicating the location of imminent failure and showed remarkable agreement with the FE predictions in regards to both strain patterns and quantitative strain values. Interestingly, the DVC and FE assessments of F7 show that the strains in the regions of high tensile strain at the inferior aspect of the neck and high compressive strain at the superior aspect of the neck are both near the critical strain values of 0.62% and -1.04% for tension and compression, respectively. Hence, the femoral neck fracture may involve a complicated mix of tensile and compressive fracture.

353

Internal strains in bone have previously been measured using DVC [28] based on micro-CT images. However, in our study the analysis was based on images from a clinical CT-scanner. Prior to this study it was not clear that such an analysis would be possible. The feasibility of using clinical CT scans opens up the possibility of measuring internal bone strains also in patients and enables a great range of possible applications.

359

This study demonstrated that from an FE assessment of a patient's femoral structure it is possible to evaluate if the patient is prone to suffer a neck or an intertrochanteric fracture, thus, a hip protector, exercises or drug therapy that protects against the specific fracture type can be chosen. Also the study developed a novel DVC technique based on clinical CT scans which may have substantial clinical significance. The technique may be applied to measure the strains around

365 implants in patients, thereby monitoring the status of the fixation as part of patient follow-up or

366 aid in the development of implants resulting in more benign stresses around the implant. Another

367 major use of the DVC technique may be the assessment of the bone strains in patients under

368 abnormal loading caused by, for example arthritis or bone deformities, providing unique

369 information for the understanding and subsequent treatment of these pathologies.

370

371 **AUTHOR'S CONTRIBUTIONS**

372 Research design: MIZR, BP, JC, and UNH. Data analysis and interpretation: MIZR, CS, BP,

373 RJvA, ABell, MK, AB, RB, OB, JC, and UNH. Drafting of manuscript: MIZR, BP, RJvA, OB,

374 and UNH. Revision of manuscript: CS, ABell, MK, AB, RA, and JC. All authors have read and

375 approved this manuscript.

376

381 **REFERENCES**

382 1. AIHW. 2010. The problem of osteoporotic hip fracture in Australia. Buletin no 76 CAT.

383   no. AUS121. Canberra: AIHW.

384 2. Evans PJ, McGrory BJ. 2002. Fractures of the proximal femur. Hosp Physician 38:30-38.

385 3. Heinonen A, Mantynen J, Kannus P, et al. 2012. Effects of high-impact training and

386   detraining on femoral neck structure in premenopausal women: a hip structural analysis of

387   an 18-month randomized controlled exercise intervention with 3.5-year follow-up.

388   Physiother Can 64:98-105.

389 4. Nikander R, Kannus P, Dastidar P, et al. 2009. Targeted exercises against hip fragility.

390   Osteoporos Int 20:1321-1328.

391 5. Keaveny TM, Hoffmann PF, Singh M, et al. 2008. Femoral bone strength and its relation

392   to cortical and trabecular changes after treatment with PTH, alendronate, and their

393   combination as assessed by finite element analysis of quantitative CT scans. J Bone Miner

394   Res 23:1974-1982.

395 6. Hong TH, Moon KH. 2015. Localized femoral BMD T-scores according to the fracture

396   site of hip and the evaluation of the sensitivity of the high risk group designated by FRAX®

397   in hip fracture patients. Osteoporosis and Sarcopenia 1:109-114.

398 7. Maeda Y, Sugano N, Saito M, et al. 2011. Comparison of femoral morphology and bone

399   mineral density between femoral neck fractures and trochanteric fractures. Clin Orthop

400   Relat Res 469:884-889.

401 8. Koivumaki JE, Thevenot J, Pulkkinen P, et al. 2010. Does femoral strain distribution

402   coincide with the occurrence of cervical versus trochanteric hip fractures? An experimental

403   finite element study. Med Biol Eng Comput 48:711-717.

404 9. Pulkkinen P, Eckstein F, Lochmuller EM, et al. 2006. Association of geometric factors and

405   failure load level with the distribution of cervical vs. trochanteric hip fractures. J Bone

406   Miner Res 21:895-901.

407 10. Gomez-Benito MJ, Garcia-Aznar JM, Doblare M. 2005. Finite element prediction of proximal femoral fracture patterns under different loads. J Biomech Eng 127:9-14.

409 11. Gnudi S, Ripamonti C, Lisi L, et al. 2002. Proximal femur geometry to detect and distinguish femoral neck fractures from trochanteric fractures in postmenopausal women. Osteoporos Int 13:69-73.

412 12. Keyak JH, Rossi SA, Jones KA, et al. 2001. Prediction of fracture location in the proximal femur using finite element models. Med Eng Phys 23:657-664.

414 13. Fox KM, Magaziner J, Hebel JR, et al. 1999. Intertrochanteric versus femoral neck hip fractures: differential characteristics, treatment, and sequelae. J Gerontol A Biol Sci Med Sci 54:M635-640.

417 14. Duboeuf F, Hans D, Schott AM, et al. 1997. Different morphometric and densitometric parameters predict cervical and trochanteric hip fracture: the EPIDOS Study. J Bone Miner Res 12:1895-1902.

420 15. Mautalen C, Vega E, Einhorn T. 1996. Are the etiologies of cervical and trochanteric hip fractures different? Bone 18:S133-S137.

422 16. Mautalen C, Vega E. 1993. Different characteristics of cervical and trochanteric hip fractures. Osteoporos Int 3:102-105.

424 17. Bessho M, Ohnishi I, Matsumoto T, et al. 2009. Prediction of proximal femur strength using a CT-based nonlinear finite element method: differences in predicted fracture load and site with changing load and boundary conditions. Bone 45:226-231.

427 18. Pottecher P, Engelke K, Duchemin L, et al. 2016. Prediction of hip Failure load: In Vitro Study of 80 Femurs Using Three Imaging Methods and Finite Element Models—The European Fracture Study (EFFECT). Radiology 280:837-847.

430   19.   Wakao N, Harada A, Matsui Y, et al. 2009. The effect of impact direction on the fracture

431   load of osteoporotic proximal femurs. Med Eng Phys 31:1134-1139.

432   20.   Keyak JH, Rossi SA, Jones KA, et al. 1997. Prediction of femoral fracture load using

433   automated finite element modeling. J Biomech 31:125-133.

434   21.   Ford CM, Keaveny TM, Hayes WC. 1996. The effect of impact direction on the structural

435   capacity of the proximal femur during falls. J Bone Miner Res 11:377-383.

436   22.   Lotz J, Cheal E, Hayes W. 1995. Stress distributions within the proximal femur during gait

437   and falls: implications for osteoporotic fracture. Osteoporos Int 5:252-261.

438   23.   Courtney AC, Wachtel EF, Myers ER, et al. 1994. Effects of loading rate on strength of

439   the proximal femur. Calcif Tissue Int 55:53-58.

440   24.   de Bakker PM, Manske SL, Ebacher V, et al. 2009. During sideways falls proximal femur

441   fractures initiate in the superolateral cortex: evidence from high-speed video of simulated

442   fractures. J Biomech 42:1917-1925.

443   25.   Dragomir-Daescu D, Op Den Buijs J, McEligot S, et al. 2011. Robust QCT/FEA models

444   of proximal femur stiffness and fracture load during a sideways fall on the hip. Ann Biomed

445   Eng 39:742-755.

446   26.   Hussein AI, Mason ZD, Morgan EF. 2013. Presence of intervertebral discs alters observed

447   stiffness and failure mechanisms in the vertebra. J Biomech 46:1683-1688.

448   27.   Madi K, Tozzi G, Zhang QH, et al. 2013. Computation of full-field displacements in a

449   scaffold implant using digital volume correlation and finite element analysis. Med Eng

450   Phys 35:1298-1312.

451   28.   Bay BK, Smith TS, Fyhrie DP, et al. 1999. Digital volume correlation: Three-dimensional

452   strain mapping using X-ray tomography. Experimental Mechanics 39:217-226.

453 29. Tuncer M, Cobb JP, Hansen UN, et al. 2013. Validation of multiple subject-specific finite
454   element models of unicompartmental knee replacement. Med Eng Phys 35:1457-1464.

455 30. Bayraktar HH, Morgan EF, Niebur GL, et al. 2004. Comparison of the elastic and yield
456   properties of human femoral trabecular and cortical bone tissue. J Biomech 37:27-35.

457 31. Keyak JH, Rossi SA. 2000. Prediction of femoral fracture load using finite element models:
458   an examination of stress- and strain-based failure theories. J Biomech 33:209-214.

459 32. Massoud EI. 2010. Fixation of basicervical and related fractures. Int Orthop 34:577-582.

460 33. Geertzen J. 2012. Inter-Rater Agreement with multiple raters and variables. Retrieved
461   December 5, 2016, from https://nlp-mlio/jg/software/ira/.

462 34. Cody DD, Gross GJ, Hou FJ, et al. 1999. Femoral strength is better predicted by finite
463   element models than QCT and DXA. J Biomech 32:1013-1020.

464 35. Orwoll ES, Marshall LM, Nielson CM, et al. 2009. Finite element analysis of the proximal
465   femur and hip fracture risk in older men. J Bone Miner Res 24:475-483.

466 36. Cheng XG, Lowet G, Boonen S, et al. 1997. Assessment of the strength of proximal femur
467   in vitro: relationship to femoral bone mineral density and femoral geometry. Bone 20:213-
468   218.

469 37. Dretakis EK, Papakitsou E, Kontakis GM, et al. 1999. Bone mineral density, body mass
470   index, and hip axis length in postmenopausal cretan women with cervical and trochanteric
471   fractures. Calcif Tissue Int 64:257-258.

472 38. Pulkkinen P, Jamsa T, Lochmuller EM, et al. 2008. Experimental hip fracture load can be
473   predicted from plain radiography by combined analysis of trabecular bone structure and
474   bone geometry. Osteoporos Int 19:547-558.

475   39.   Nishiyama KK, Gilchrist S, Guy P, et al. 2013. Proximal femur bone strength estimated by

476   a computationally fast finite element analysis in a sideways fall configuration. J Biomech
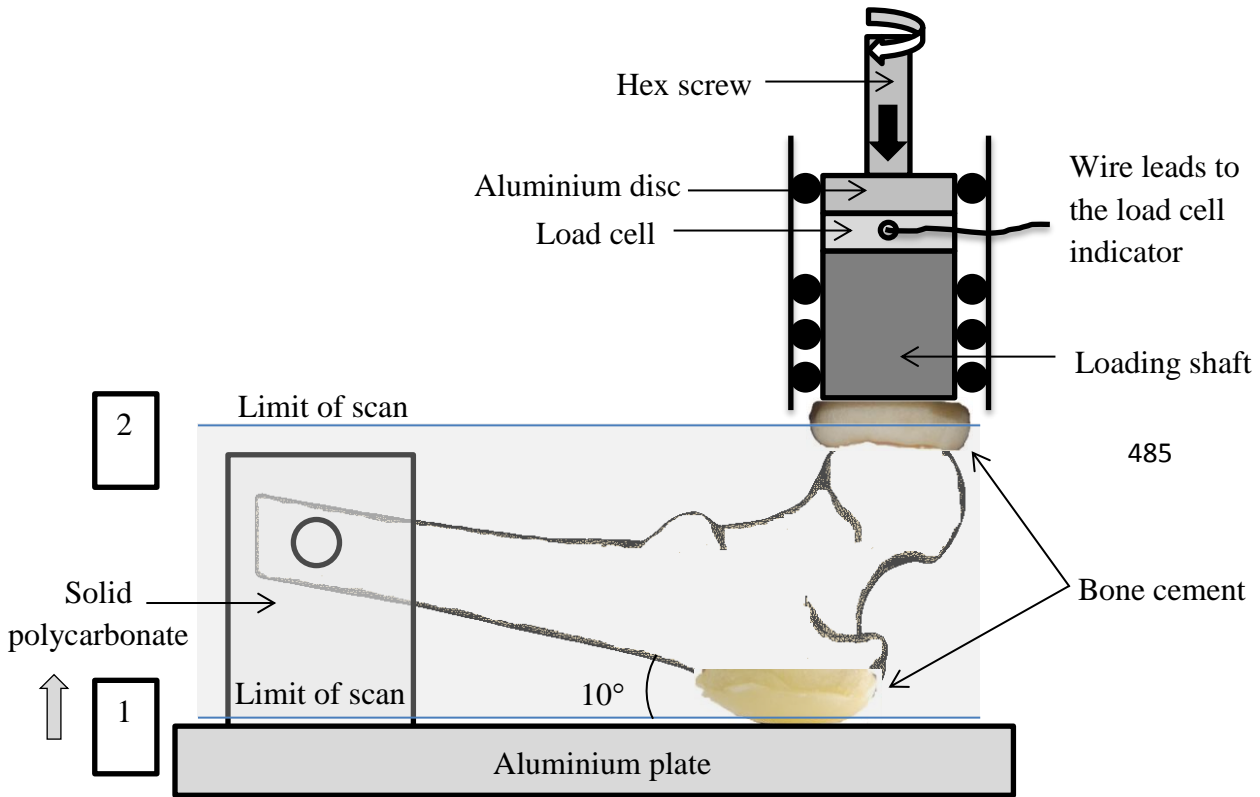
477   46:1231-1236.

478

479

480

481

Hex screw

Aluminium disc

Load cell

Wire leads to the load cell indicator

Loading shaft

Limit of scan

2

485

Solid polycarbonate

Bone cement

1

Limit of scan

10°

Aluminium plate

487

Figure 1 – Schematic diagram of the mechanical test-setup for Part 2 of the mechanical testing which is carried out within a CT scanner. The CT scanning started from position 1 moving to position 2. The resulting scan volume contained no metal components and no metal artifacts. For Part 1 of the mechanical testing the fixture above was placed within a standard Instron Mechanical testing machine and the load introduced via the cross head and load cell of the Instron (replacing the load device shown in the upper part of the figure). Also, for part 1 the bottom Aluminium plate was replaced by an x-y table.
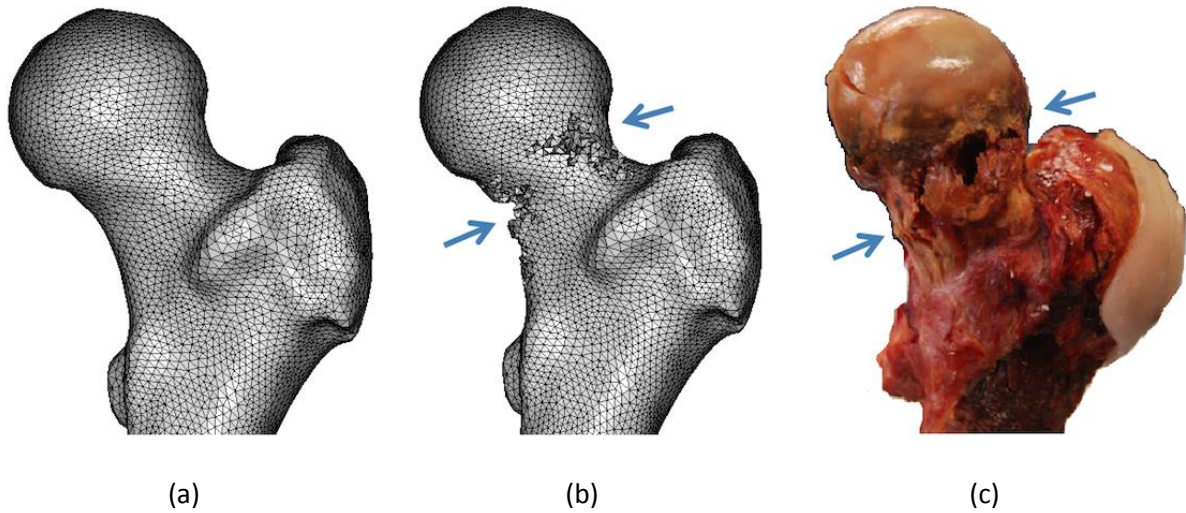
498

499

500

501

502

(a)   (b)   (c)

Figure 2 – (a) FE meshed model before initiation of fracture and (b) the same model with deleted

elements at the point of ultimate fracture load and (c) the actual fractured femur that was simulated

(specimen M2). Both the FE simulation and the experimental test showed a neck type fracture.
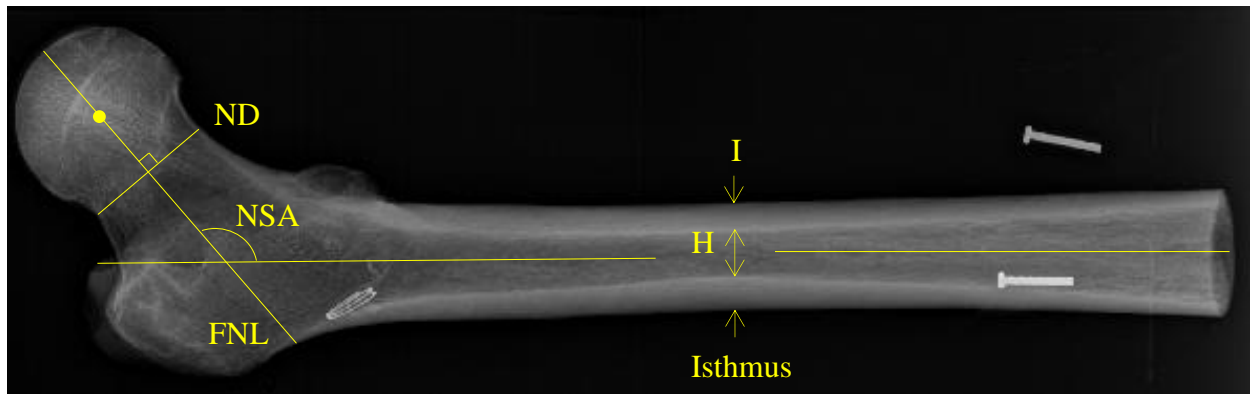
509

510

511

512

513

514

515

516

517

518

519

520

521

522

523

524

Figure 3 – Geometrical parameters of the femur. ND = width of femoral neck at its most narrow

point, FNL = femoral neck length, NSA = neck shaft angle measured as angle between the femoral

neck and the femoral shaft axes, and the cortical index (CI) at the femoral isthmus that equals to

the ratio of the femoral diaphyseal diameter (I) minus the intramedullary canal diameter (H) over

the femoral diaphyseal diameter; C = (I – H) / I

530

531
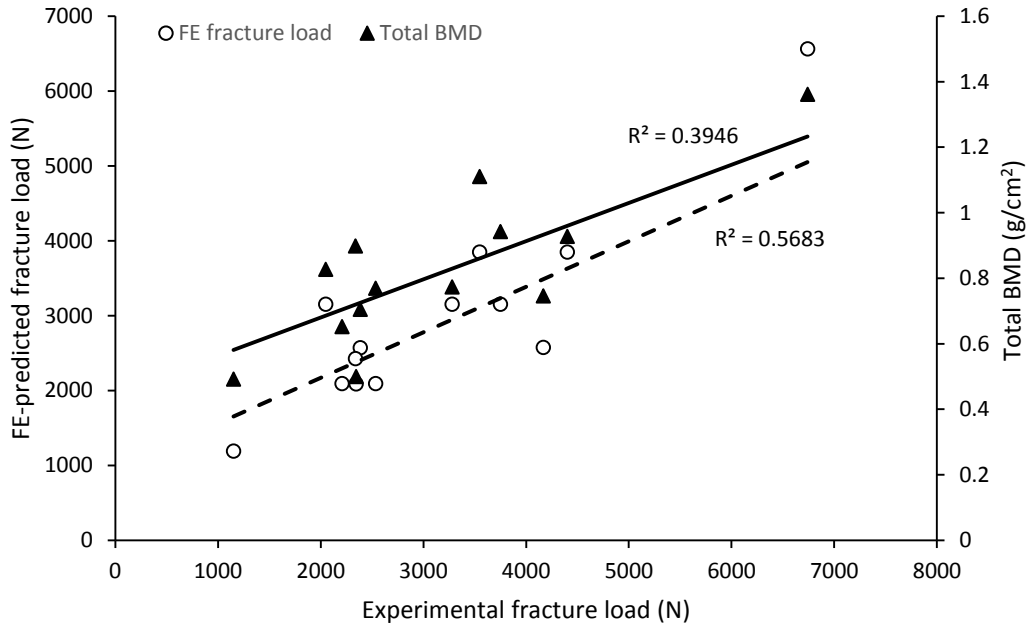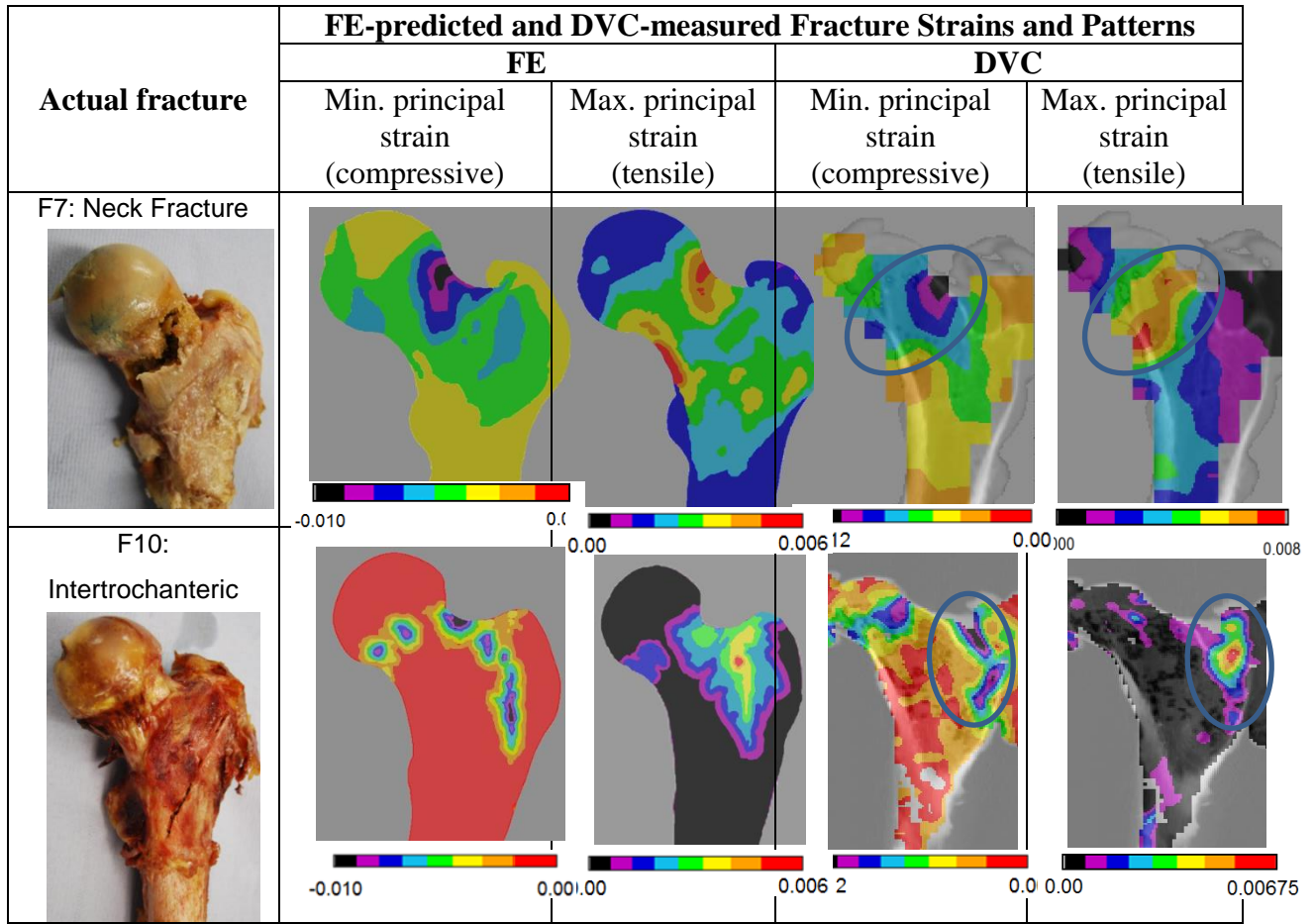
532

533

534

535

536

537

538

539

540

541

Figure 4 - The ability of FE to predict the actual (the experimental) fracture load compared to the

ability of DXA-based BMD to predict the actual fracture load. Dashed line relates to FE fracture

load data, solid line to BMD data.

545

546

547

548

	FE-predicted and DVC-measured Fracture Strains and Patterns			
Actual fracture	**FE**		**DVC**	
	Min. principal strain (compressive)	Max. principal strain (tensile)	Min. principal strain (compressive)	Max. principal strain (tensile)
F7: Neck Fracture				
F10: Intertrochanteric				

549

Figure 5 – Comparison of the experimentally observed fractures to the FE-predicted strain and fracture patterns as well as to the DVC-measured strains. Top row: Femur F7 exhibiting a femoral neck fracture. Bottom row: Femur F10 exhibiting an intertrochanteric fracture. High strain concentrations (circled) were apparent in regions where the femoral failure occurred and reflected the different fracture modes. Note, the DVC image of femur F10 is shown in an oblique view to better demonstrate the strain concentrations.

556

557   **Table 1** – Predicted and experimental fracture load and type listed in order of experimental fracture

558   load and according to gender.

Specimen	Total BMD (g/cm²)	Fracture load (N)		Fracture type Observations in brackets.	
		Experiment	FE	Experiment	FE
F1	0.75	4166	2575	(Subcap oblique/basicervical) Neck	(Basicervical) Intertrochanteric
F2	0.94	3748	3154	(Subcapital) Neck	(Transcervical/basicervical) Neck
F3	0.77	3278	3153	(Basicervical/intertrochanteric) Intertrochanteric	(Basicervical/intertrochanteric) Intertrochanteric
F4	0.77	2534	2094	(Basicervical/intertrochanteric) Intertrochanteric	(Basicervical/transcervical) Intertrochanteric
F5	0.71	2382	2573	(Subcapital) Neck	(Transcervical) Neck
F6	0.50	2342	2091	(Basicervical/intertrochanter) Intertrochanteric	(Basicervical/intertrochanteric) Intertrochanteric
F7*	0.90	2339*	2425	(Transcervical) Neck	(Subcapital/basicervical) Neck
F8	0.65	2205	2091	(Basicervical) Intertrochanteric	(Cervical/basicervical) Neck
F9	0.83	2049	3153	(Basicervical) Intertrochanteric	(Trochanteric/basicervical) Intertrochanteric
F10*	0.49	1151*	1190	(Intertrochanteric/trochanteric) Intertrochanteric	(Intertrochanteric/trochanteric) Intertrochanteric
M1	1.36	6739	6565	(Intertrochanteric/basicervical) Intertertrochanteric	(Basicervical) Intertrochanteric
M2	0.93	4399	3850	(Subcapital/transcervical) Neck	(Cervical) Neck
M3	1.11	3547	3849	(Basicervical/intertrochanteric) Intertrochanteric	(Basicervical) Intertrochanteric
M4	1.00	-	3153	(Subcapital/transcervical) Neck	(Cervical + basicervical) Neck

559   *the recorded loads prior to failure (specimens used for DVC experiments)

560

561

562

563

564

565 **Table 2** - Summary of the FE-predicted fractures and the observed fractures.

		Experimental	
		Neck	Intertrochanteric
FE	Neck	5	1
	Intertrochanteric	1	7

566

567

568

569

570

571

572

573

574

575

576

577

578

579

580

581

582

583

584

585

586

587

Table 3 – Comparison of specimen characteristics between fracture types.

588

| | Neck fracture (n = 6) | Intertrochanteric fracture (n = 7) | p-value | Females only | | |
				Neck fracture (n=4)	Intertrochanteric fracture (n=6)	p-value
Female/male	4/2	6/1	0.56	4/0	6/0	n/a
Age (years)	73.8 ± 14.1	64.3 ± 13.6	0.24	76.8 ± 9.0	68.0 ± 10.4	0.21
Exp. Femoral strength (N)	3407 ± 984	2444 ± 797	0.09	3159 ± 938	2260 ± 692	0.12
Height (cm)	168.5 ± 8.4	163 ± 7.5	0.21	163.5 ± 3.1	160.2 ± 4.4	0.23
Weight (kg)	67.5 ± 24.2	74.6 ± 31.8	0.67	72.5 ± 29.6	72.0 ± 34.1	0.98
BMI	24.1 ± 9.6	27.9 ± 11.2	0.53	27.0 ± 10.9	27.7 ± 12.2	0.93
BMD at Neck (g/cm^2)	0.824 ± 0.092	0.669 ± 0.166	0.08	0.782 ± 0.092	0.624 ± 0.126	0.07
BMD at Wards (g/cm^2)	0.595 ± 0.064	0.503 ± 0.191	0.27	0.566 ± 0.040	0.445 ± 0.126	0.07
BMD Great Trochanter (g/cm^2)	0.729 ± 0.167	0.555 ± 0.185	0.11	0.649 ± 0.142	0.493 ± 0.090	0.07
Total BMD (g/cm^2)	0.870 ± 0.117	0.732 ± 0.213	0.19	0.823 ± 0.115	0.669 ± 0.146	0.12
Isthmus CI	0.59 ± 0.05	0.58 ± 0.07	0.83	0.57 ± 0.05	0.57 ± 0.08	0.90
Neck diameter (cm)	3.2 ± 0.3	3.2 ± 0.3	0.72	3.1 ± 0.2	3.1 ± 0.2	0.96
FNL (cm)	9.9 ± 0.7	9.9 ± 0.7	0.98	9.5 ± 0.3	9.7 ± 0.5	0.51
NSA (°)	127 ± 4.5	125 ± 5.6	0.72	124 ± 3.6	124 ± 3.4	0.80